Separation and Purification Technology 306 (2023) 122625

Contents lists available at ScienceDirect

Separation and Purification Technology

journal homepage: www.elsevier.com/locate/seppur

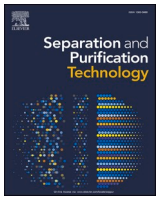

The novel SiO_2-decorated highly robust waste-derived activated carbon with homogeneous fluidity for the CO_2 capture process

Milad Iranvandi [a], Maryam Tahmasebpoor [a,*], Babak Azimi [a], Mohammad Heidari [a,b], Covadonga Pevida [c,*]

[a] Faculty of Chemical & Petroleum Engineering, University of Tabriz, PO Box 51666-16471, Tabriz, Iran
[b] Department of Chemical Engineering, Faculty of Engineering, University of Kurdistan, Sanandaj, Iran
[c] Instituto de Ciencia y Tecnología del Carbono, INCAR (CSIC), Francisco Pintado Fe, 26, 33011 Oviedo, Spain

ARTICLE INFO

Keywords:
CO_2 capture
Fluidization
Date seeds
Activated carbon
Biomass
Silica nanoparticles

ABSTRACT

Biomass-derived activated carbon (AC) is considered auspicious for alleviating various environmental pollutants. We reported the usage of a developed biomass-based AC as a potential adsorbent for CO_2 uptake applications to overcome global warming. In this paper, AC was successfully synthesized from a highly-used fruit in the middle east, date seeds, and chemically activated by KOH to boost CO_2 uptake activity. The fluidization behavior was tested and improved through a dry-mixing route with fluidizable nanopowder. To assess the impact of utilizing the chemical activator and easily-fluidizable compound, CO_2 capture efficiency and fluidity of the raw and promoted adsorbent were evaluated and compared with commercial and other date-derived ACs. The original and modified ACs were characterized via SEM, EDS, BET, FTIR, and TG analysis; the KOH-promoted AC possessed a more fluffy-like configuration and a higher surface area of about 595.94 m^2/g. Based on the TG analyses, 94% and 67% higher average CO_2 capture capacity was recorded for KOH-promoted ACs compared to the original and commercial adsorbents. The KOH-promoted ACs and SiO_2-covered counterparts fluidization's performance was assessed under 15 vol% CO_2 balanced with N_2 gas. Fluidization experiments proved the positive effect of employing hydrophobic silica nanoparticles (NPs) to develop the fluidity of the synthesized activated carbon. After mixing with 2.5 wt% SiO_2 NPs, the SiO_2-decorated modified ACs presented a 45% higher bed expansion ratio associated with a homogeneous and bubbleless fluidized regime.

1. Introduction

Our world has impetuously suffered from distasteful environmental crises, mainly the shortage of drinkable water and particularly global warming [1,2]. CO_2 gas as the most substantial anthropogenic greenhouse gas leads to severe increases in global warming and climate changes worldwide [3,4]. Hence, carbon capture for utilization and storage (CCUS) technologies have been recognized as the most promising key to tackling the detrimental effects of released CO_2 [5,6]. Currently, three principal CO_2 capture technologies, pre-combustion, oxy-fuel combustion, and post-combustion methods are widely exploited in several fields [7,8]. Among post-combustion capture CO_2 technologies, including absorption [9], membrane separation [10,11], calcium looping technology [12], cryogenic fractionation [13], ionic liquid [14], and adsorption [15], solid-state adsorbents have grabbed focus due to the ability to be retrofitted for short to medium term without encountering any significant technology risks or changes [1,16,17]. There are numerous types of solid adsorbents, namely zeolites [18], porous crystalline frameworks [19], fluffy-like polymers [20], metal oxides [21,22], and carbon-based adsorbents [23]. Among the mentioned solid adsorbents, environmentalists have put the focus on low-cost activated carbon adsorbents due to their favorable features: widely accessible, easily-preparation, reversibility in cycles at low adsorption and desorption temperatures, hydrophobicity, promising porosity, chemical resistivity to alkaline and acidic conditions, and thermal and mechanical stability [24,25]. Nanostructured activated carbons are usually prepared from the pyrolysis of carbonaceous materials in an O_2-free atmosphere that leads to the removal of their volatile compounds. It is worth noting that today, carbon-based nanoparticles have many applications in industry and the environment, such as improving transmission phenomena in power plants [26–28]. The textural properties of the chosen carbon precursor, typically coal, peat,

* Corresponding authors.
E-mail addresses: tahmasebpoor@tabrizu.ac.ir (M. Tahmasebpoor), cpevida@incar.csic.es (C. Pevida).

https://doi.org/10.1016/j.seppur.2022.122625
Received 22 September 2022; Received in revised form 31 October 2022; Accepted 8 November 2022
Available online 21 November 2022

lignite, wood, wheat straw, rice husk, date seeds, waste bamboo, or fruit bunch [29,30], the synthesis approach, activation method, and the type of activating agent play a vital role in the capture performance of the prepared activated carbon.

Physical and chemical activation methods have been employed as two main approaches to boost the surface area, multi-channel pores, and adsorption efficiency. [31,32]. It has been declared that chemical activation is preferable to physical activation due to several benefits, including providing a suitable texture for the final product, less activation time, and higher yield [33]. During the chemical activation process, starting materials are impregnated with a dehydrating agent such as potassium hydroxide (KOH), sodium hydroxide (NaOH), phosphoric acid (H_3PO_4), sulfuric acid (H_2SO_4), and zinc chloride ($ZnCl_2$) followed by pyrolysis and activation stages to form the final product [31,32]. In an interesting research, the activated carbon derived from bee-collected pollens was chemically activated with KOH through the wet impregnation technique, using a KOH/pollen mass ratio of 3:1. The novel adsorbent showed a remarkable CO_2 sorption capacity of 3.42 mmol CO_2/g adsorbent at 298 K and 1 bar [34]. Serafin et al. [35] prepared the activated carbon from Lumpy Bracket by KOH-activation to enhance its sorption activity. The chemical KOH activation on the corresponding activated carbon resulted in the high CO_2 uptake potentials of 4.62 and 7.15 mmol CO_2/g adsorbent under 1 bar and at 298 and 273 K, respectively.

Phoenix dactylifera, commonly known as date palm, is a flowering plant cultivated in arid and semi-arid regions such as northern Africa, the Middle East, and South Asia. Date palm is cultivated for its edible sweet fruit called dates, while the seeds are discarded as agricultural wastes. Recently, palm date seeds have been utilized for making healthy drinks and fabricating beneficial products like activated carbon [36,37]. Ogungbenro et al. [31] synthesized date-seed-obtained ACs via CO_2 activation and pyrolysis. With the sample being pyrolyzed at 800 °C and activated at 900 °C, its CO_2 capture capacity increased by 32% at ambient temperature. Another investigation conducted by Ogungbenro et al. [32] screened the effect of H_2SO_4-activation on the adsorption capability of activated carbons synthesized from palm date seeds via the impregnation method by considering diverse activation temperatures (600, 700, 800, and 900 °C) and impregnation ratios of 0.5:1, 1:1, and 2:1. Among the samples, the adsorbents developed at the activation temperature of 700 and impregnation ratio of 1:1 presented the highest CO_2 capture capacity of 78.71 mg CO_2/ g adsorbent at 20 °C. To confirm the superior activity of date seeds to prepare ACs, Mumtaz et al. [38] synthesized activated carbons utilizing five different waste biomass materials using chemical activation. They demonstrated that the activated carbon from date seeds showed a superior capture capacity of ~5.8 mmol/g at 0 °C. The summary of conducted investigations on developing chemically activated carbons from biomass materials for a low-temperature CO_2 capture process is included in Table 1.

The appropriate fluidity of the fine particles plays a crucial role in the industrialization of the CO_2 capture process, commonly performed in fluidized bed reactors [39]. Activated carbon powders that belong to the Geldart C classification have a very cohesive nature showing inappropriate fluidization behavior [40]. Strong interactions between activated carbon fine particles lead to the formation of numerous compact agglomerates, usually stable and nondisruptive to gas flow [45]. The heterogeneous fluidization behavior of fine powder particles, arising from interparticle adhesion forces, causes the appearance of permanent gas channels and slugs, leading to the non-uniform flow gas distribution through the bed, inefficient particles-gas contact, and reduced CO_2 capture efficiency [41,42]. Thus, homogeneous fluidity is required to hinder bubble-forming across the bed and boost the gas-solid contact efficiency [43,44]. Based on the findings, among all improvement methods, the physical mixing of easily-fluidizable particles with hard-to-fluidized fine particles resulted in more improvement in the fluidization quality. Valverde et al. [45] evaluated the effect of merging easy-fluidizable SiO_2 nanoparticles (NPs) with hard-to-fluidize $Ca(OH)_2$ fine particles on their fluidization quality and CO_2 capture activity. The considered modification method served to significantly reduce the interparticle cohesion forces between $Ca(OH)_2$ nanoparticles leading to the homogeneous fluidization behavior and boosting the CO_2 capture capacity of $Ca(OH)_2$ in fluidized bed reactors. Amjadi et al. [46] added Aerosil R972 nanoparticles onto the surface of $Ca(OH)_2$ particles to

Table 1
Summary of the performance of chemically activated carbon adsorbents applied in the CO_2 capture process in recent literature.

Raw material (source)	Activation					S_{BET} (m^2/g)	V_T (cm^3/g)	Adsorption conditions			Sorption capacity (mmol/g)	Ref
	Time (h)	T (°C)	Chemical activator	Washing agent	Activator/ precursor (wt%)			T (°C)	P_{CO2}(bar)	CO_2 vol%		
Task-specific ionic liquid	2-Jan	600	KOH	HCl/ NH_4OH	1.5:1	1317	0.64	25	1	100	5.39	[47]
Starch	0.17	700	KOH	HCl/H_2O	04:01	1636	0.51	25	1	100	3.84	[48]
Pomegranate peels	1	700	KOH	HCl/H_2O	01:01	585	0.28	25	1	100	4.11	[49]
Piptoporus betulinus	1	700	KOH	HCl/H_2O	01:01	1267	0.45	25	1	100	3.53	[49]
Trametes versicolor (L.) Lloy	1	700	KOH	HCl/H_2O	01:01	1346	0.57	25	1	100	3.29	[49]
Mistletoe branches	1	700	KOH	HCl/H_2O	01:01	1111	0.55	25	1	100	2.54	[49]
Carrot peels	1	700	KOH	HCl/H_2O	01:01	1379	0.58	25	1	100	4.18	[49]
Kiwi fruit peels	1	700	KOH	HCl/H_2O	01:01	1381	0.62	25	1	100	2.8	[49]
Fern leaves	1	700	KOH	HCl/H_2O	01:01	1593	0.74	25	1	100	4.12	[49]
Sugar, beet pulp	1	700	KOH	HCl/H_2O	01:01	1263	0.62	25	1	100	2.88	[49]
Glucose	1.5	800	KOH	HCl/H_2O	01:01	862	0.44	25	1	100	4.3	[50]
Rice husk char	1	900	CO_2	H_2O	–	1097	0.83	25	1.013	100	3.1	[51]
Starch	1	700	KOH	HCl/H_2O	03:01	1283	0.686	25	1	100	4.24	[52]
Tea seed shell	2	700	KOH	HCl/H_2O	04:01	1503.2	0.64	25	1	100	3.15	[53]
Black locust	1.5	830	KOH	HCl/H_2O	06:01	2064	0.98	25	1	100	3.75	[54]
Sugarcane bagasse	0.5–1	600	KOH	HCl/H_2O	02:01	1113	0.508	25	1	100	4.8	[55]
Bamboo	1.5	600	KOH	HCl/H_2O	03:01	–	–	25	1	100	4.5	[56]
Agaricus (fungus)	1	700	KOH	–	01:01	1600	0.72	25	1	100	3.5	[57]
Potato starch	1	700	KOH	HCl/H_2O	04:01	2190	1.01	25	1.013	100	3.5	[58]
Cellulose	1	700	KOH	HCl/H_2O	04:01	2370	1.08	25	1.013	100	3.5	[58]
Eucalyptus sawdust	1	650	KOH	HCl/H_2O	02:01	1380	0.67	25	1.013	100	4.7	[58]
Empty fruit bunch	0.5	800	KOH	HCl/H_2O	05:01	2510	1.05	25	1	100	3.71	[59]
Jujun grass	1	700	KOH	HCl/H_2O	04:01	3144	1.56	25	1	100	4.1	[60]
Camellia japonica	1	700	KOH	HCl/H_2O	02:01	1150	0.56	25	1	100	5	[60]

enhance their fluidizability, and scrutinized the effect of three parameters, $Ca(OH)_2$ powder sieved size, silica NPs sieved size, and SiO_2 weight percentage, on the fluidization quality. They indicated that the sieve size of the CaO-based adsorbents does not have an appreciable impact on the bed expansion ratio in contrast to silica NPs sieved size and SiO_2 weight percentage.

Due to the comprehensively reviewed investigations, most research activities demonstrated the high CO_2 sorption capability of biomass-derived ACs and announced the positive effect of KOH activation on their sorption activity. To the best of our knowledge, no consideration has been paid to developing easily-fluidizable ACs derived from date seeds for the CO_2 capture process. On the other hand, the fluidization quality of ACs is the most determinant parameter for the industrialization of CO_2 adsorbents in fluidized beds, but it is not well understood as yet. This investigation addresses, for the first time, the flowability of the most efficient KOH-activated AC. It was evaluated in a purposely designed lab-scale fluidized bed system and enhanced with easily fluidizable SiO_2 NPs as innovative additives.

The carbon-based adsorbent was prepared through pyrolysis of cost-effective and widely available date seeds. Then, the abovementioned adsorbent was chemically activated by the KOH solution. In addition to multicyclic CO_2 uptake performance during different cycles, the impact of adsorption temperature and CO_2 concentration of inlet gas on the ultimate uptake potential of the adsorbents was assessed thoroughly. The synthesized AC was mixed with 2.5 wt% SiO_2 and its fluidization and adsorptive behavior were evaluated in the lab-scale fluidized-bed system. It is worth noting that the CO_2 capture performance of fluidizable ACs has not been previously studied in the literature. As a novel finding, highly efficient and fluidizable SiO_2-merged ACs derived from date seeds were developed.

2. Experimental

2.1. Materials

Local date seeds were utilized as the starting material for the fabrication of the activated carbon adsorbents. Commercial activated carbon (CAC) was also purchased (from Arman Sina, Iran) to compare with the activated carbon synthesized in this work. Potassium hydroxide (KOH from Merck, Germany) was purchased as the chemical activating reagent. Distilled water (H_2O from Arman Sina, Iran) and hydrochloric acid (HCl from Arman Sina, Iran) were utilized for washing the compounds and solubilization within synthetic processes. Hydrophobic nanostructured amorphous fumed silica (Aerosil® R972 from Evonik, Germany), which possesses a BET surface area of 110 ± 20 m^2/g, primary particle size of 16 nm, and particle density of 1200 kg/m^3, was employed as an auxiliary substance with the aim of enhancing the fluidizability of the synthesized activated carbon.

2.2. Preparation

Characteristics of the commercial and synthesized activated carbons are presented in Table 2. Chemical activation reagent was added to the carbon-based adsorbents with a 1:1 weight ratio. The obtained ACs from the pyrolysis of date seeds, chemically modified ACs with KOH, and physically modified KOH-promoted ACs with 2.5 wt% SiO_2 NPs were denoted as D, D_{KOH}, and $S_{2.5}D_{KOH}$, respectively.

2.2.1. Preparation of activated carbon from waste biomass materials

Firstly, date seeds were washed with distilled water to remove the excess elements. Secondly, these seeds were dried in an oven at 600 °C for 2 h. Dried seeds were crushed and sieved to obtain particles with the size in the range of 1–3 mm. A 3 mol/L solution of KOH was employed separately in the impregnation of the proper amount of obtained sieved particles (10 g) at 30 °C for 24 h. 10 g of resulting sieved particles were impregnated with a fixed ratio of KOH. Impregnated samples were dried in airflow at 85 °C for 24 h and then were put into a muffle furnace at 600 °C for 2 h to carry out carbonization and complete the activation. The prepared samples were washed with 0.1 mol/L HCl and distilled water to remove surplus chemical activating reagent. Washed samples were dried at 100 °C for 24 h and then were sieved to obtain the final products. Schematic of the activated carbon production process is presented in Fig. 1.

2.2.2. Physical mixing with additives

At first, auxiliary silica powder was sieved using a 150 μm sieve placed on a shaker to eliminate excessively large agglomerates. Secondly, synthesized adsorbents and auxiliary materials were mixed for 30 min in dry conditions to prepare the enhanced adsorbents. The easily fluidizable silica nanopowders serve as dispersants and carriers of the cohesive adsorbent particles, enhancing the gas-solids contact efficiency between the adsorbents and the fluidizing gas. We have employed additive nanopowders in a low weight percentage of 2.5 for our experiments to alleviate the flowability of non-fluidizable ACs without decreasing their CO_2 uptake.

2.3. Apparatus

Fluidization experiments of fabricated adsorbents were carried out in a glass-made fluidized bed illustrated in Fig. 2. In each test, 4 g of adsorbent were placed in a vertically oriented cylindrical fluidized bed with 26 mm ID and 800 mm height. The fluidized bed was vibrated to remove the narrow voids between fine particles. Aiming to fluidize the synthesized adsorbents, a controlled flow containing 15 vol% CO_2 balanced with pure nitrogen (99.99%) passed the bed through a sintered porous plate distributor. The gas distributor ensured the homogeneous gas velocity through the fluidized bed. A cyclone and a high-efficiency gas filter were embedded at the end of the column to collect entrained particles of the leaving gas flow and avoid fine particles into the environment. Bed expansion ratio (H/H_0) clarified the fluidization quality of the examined adsorbents, where H_0 and H correspond to the bed height at zero and a certain superficial gas velocity, respectively [61]. To provide higher accuracy, better consistency and reproducibility in the evaluated bed expansion ratios all tested samples were initially fluidized at high gas velocities that were gradually decreased in small steps. It should be noted that all fluidization tests were performed at ambient temperature and atmospheric pressure.

2.4. Characterization

The morphology of the synthesized adsorbents (raw and activated carbon-based adsorbents) and also the mixing quality of the adsorbent

Table 2
Speciation of prepared carbon-based adsorbents.

Sample	Biomass precursor	Chemical activating reagent	Activating to precursor weight ratio	Activation temperature	BET surface area (m^2/g)	BJH pore volume (cm^3/g)	Pore diameter (nm)
CAC	–	–	–	–	264.4	0.093	2.895
D	Date seeds	–	–	–	359.6	0.141	2.885
D_{KOH}	Date seeds	KOH	1:1	600	595.94	0.475	2.217
$S_{2.5}D_{KOH}$	Date seeds	KOH	1:1	600	545.95	0.364	2.279

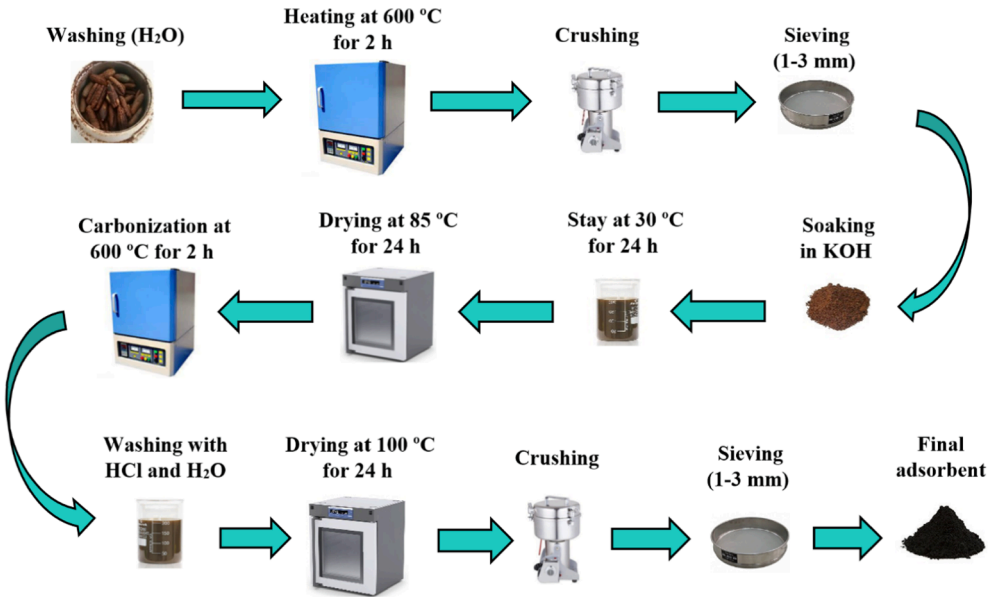

Fig. 1. Schematic for preparation of the chemically activated carbon from local date seeds.

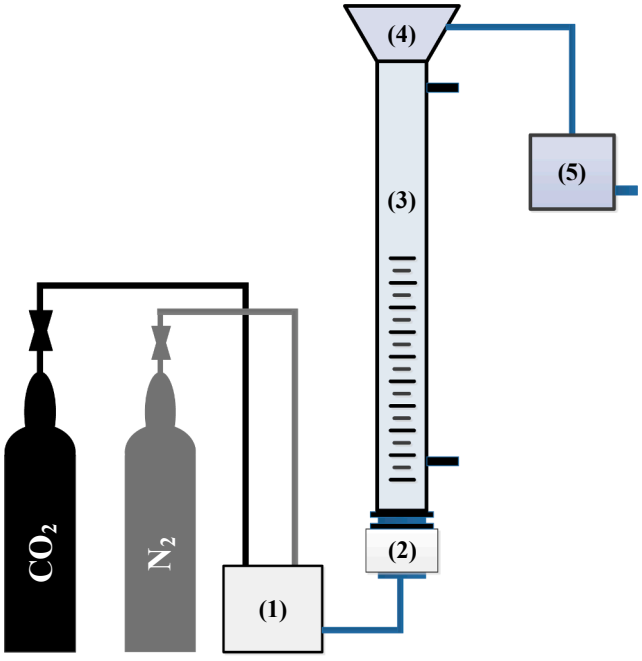

Fig. 2. Sketch of the experimental set up used for the fluidization experiments. **1**: Mixing chamber, **2**: Gas distributor chamber, **3**: Quartz reactor, **4**: Cyclone, and **5**: Particulate filter.

with auxiliary materials was assessed via scanning electron microscopy (SEM) using a 6301F HOEL (United States) microscope. The BET surface area of all the adsorbents was measured by N_2 physisorption at 77 K in a BELSORP MINI II instrument. Before the measurements, the samples were degassed under vacuum at 120 °C for 2 h. In-situ Fourier transform infrared (FTIR) spectra were performed to further analyzed the synthesized samples and identify the functional groups' present on the samples' surface [62].

2.5. CO_2 capture performance

The CO_2 uptakes of the synthesized adsorbents and their stability were evaluated through thermogravimetric analysis (TGA) in a TGA/DSC1 STARe system from Mettler Toledo over multiple adsorption/desorption cycles. About 10 mg of each adsorbent were employed in each experiment. Prior to each test, the samples were conditioned for 60 min at 120 °C in N_2 to remove physisorbed moisture and other gases such as CO_2. The CO_2 capture steps were performed at 25 and 50 °C in CO_2/N_2 flow with different gas compositions (10, 30, 50, and 90 vol% CO_2, N_2 balance) for 60 min. Desorption and regeneration of the tested samples were carried out by increasing the temperature to 120 °C with a heating rate of 10 °C/min until complete regeneration. Desorption temperature was set at 120 °C according to the samples' stability and degassing temperature in BET analysis. After complete desorption, the chamber was cooled to the adsorption temperature, and the cycle was repeated. It is worth noting that the gas flow rate was set to a small value (50 cm^3/min) to neglect external mass transfer effects. Stability experiments of the selected adsorbents were performed at 25 °C in a flow gas containing 15 vol% CO_2 in N_2. The CO_2 concentration was selected to reproduce relevant post-combustion capture conditions from point stationary sources (*e.g.*, coal power plant). The obtained results were presented in terms of the CO_2 capture capacity (mmol CO_2 captured per g of adsorbent, C_n) for each cycle, deactivation, and durability as follows:

$$C_n = \frac{m_n - m_0}{m_0} \times \frac{1000}{M_{CO_2}} \quad (1)$$

$$\text{Deactivation } (\%) = \frac{C_1 - C_n}{C_1} \times 100 \quad (2)$$

$$\text{Durability } (\%) = \frac{C_n}{C_1} \times 100 \quad (3)$$

where m_n refers to the mass of the sample at the end of the adsorption step in the n^{th} cycle, and m_0 is the mass of the sample at the end of the desorption step at 120 °C (cycle n-1). M_{CO2} is the molecular weight of CO_2 (44 g/mol).

3. Results and discussions

3.1. Characterization results

3.1.1. BET surface area and porosity analysis

The BET surface area and textural porosity characterization of the developed samples, namely pore volume and diameter, are presented in

Table 2. According to the findings, the carbon derived from date seeds indicated higher morphological and textural porosity, and the KOH-activation avenue raised the pore volume and surface area. The recorded pore volumes of 0.093, 0.141, and 0.475 cm^3/g, and average pore diameters of 2.895, 2.885, and 2.217 nm for CAC, D, and D_{KOH}, revealed the mesoporosity of the samples. Pore diameter measurement depicts that the activated sample possesses smaller pore diameters due to the formation of narrower porosity upon activation. Based on the recorded data, applying the activation process to biomass waste results in developing highly porous materials, so the surface area and pore volume of D increase from 359.6 m^2/g and 0.141 cm^3/g to 595.54 m^2/g and 0.475 cm^3/g in D_{KOH}.

3.1.2. Scanning electron microscopy (SEM) analysis

SEM images of the samples are illustrated in Error! Reference source not found.. The SEM picture of CAC exhibits a compact and non-porous morphology associated with hardly-visible narrow channels due to the blockage by fine particles. Moreover, sample D represents the dense and indiscrete morphology. The surface-resident particles appear like compressed aggregates, including a few narrow channels serving CO_2 diffusion into the adsorbent's porosity. On the other hand, D_{KOH} adsorbent consists of more morphological pores and accessible surface area than D. There is high conformity between BET and BJH values with SEM micrographs; D_{KOH} adsorbent with higher surface area and pore volume shows more surface-resident porous zones than CAC and D.

In addition, EDS analysis was carried out on the fresh samples to study the quality of components distribution on the surface, and the acquired data are reported in Table 3. The appearance of different components reveals the distribution of the surface-located elements and the completeness of the synthesis method. According to the presence of minor potassium content, 0.09 wt%, on the D_{KOH} surface, it can be concluded that the chemical activating reagent was well removed during the preparation process. The slight difference in the carbon and oxygen contents between the synthesized and commercial ACs can be attributed to the carbon precursor (See Table 3).

3.1.3. Fourier transform infrared spectroscopy (FTIR analysis)

According to the literature, in addition to the textural properties, the surface chemistry composition affects the CO_2 adsorption of activated carbon. In this regard, the FTIR technique was used to determine functional groups on the surfaces of D and D_{KOH}, plotted in Fig. 4. Comparison of the synthesized samples reveals that more functional groups, particularly volatile chemicals, were found for D compared to D_{KOH} due to the thermal treatment of D_{KOH}. Furthermore, the presented figures for D and D_{KOH} apparently demonstrate the disappearance of several peaks in ACs after the carbonization process. The broad absorbance peak in the 3600–3200 cm^{-1} region is related to moisture-induced O—H stretching and hydroxyl (-OH) groups in both samples, sensitive to activated carbons. In addition to the hydroxyl, oxygen-infused functional groups, such as carbonyl or carboxyl, are detected on the ACs surface with the peak at around 1719 cm^{-1}. With two distinct peaks at 2918 and 2853 cm^{-1} on the surface of D and $D_{KOH,}$ respectively, the presence of aliphatic C—H bonds can be deduced. Accompanied by determined peaks at 1546 and 1739 cm^{-1} for the activated adsorbent and also at 1554 and 1793 cm^{-1} for the raw sample, that correspond to the C═C bonds [63].

Table 3
Elemental analysis of the experimental samples.

Sample	Elements (wt%)							
	C	N	O	Ca	Al	Zr	Na	K
CAC	78.38	5.22	14.71	0.47	0.52	0.33	0.37	–
D	74.73	5.87	19.4	–	–	–	–	–
D_{KOH}	76.47	6.38	17.06	–	–	–	–	0.09

3.2. CO_2 capture and stability

3.2.1. Determining operational conditions

To set the optimum experimental conditions such as temperature and CO_2 partial pressure in the inlet gas flow, the CO_2 capture performance of D_{KOH} was firstly analyzed in the TGA over three consecutive adsorption/desorption cycles at 25 and 50 °C under 10, 30, 50 and 90 vol% CO_2 for the adsorption stage, and 120 °C for the desorption stage, and thier performance was reported in Table 4. The mass gain during the process (i.e., versus time) and ultimate CO_2 uptake are presented in Figs. 5 and 6, respectively. Under 10 vol% CO_2 and at 25 °C, D_{KOH} shows an average CO_2 uptake of 1.21 mmol/g, increasing up to 1.72, 2.09, and 2.7 mmol/g with the CO_2 concentration from 30, 50, to 90 vol%, respectively. As expected, the CO_2 capture increases by raising the CO_2 partial pressure in the feed stream. Consequently, the increment in adsorption temperature leads to a decrease in CO_2 uptake, so that 29% decrease in the CO_2 capture level of D_{KOH} under 90 vol% CO_2 was reported by increasing the adsorption temperature from 25 °C to 50 °C. Therefore, CO_2 uptake values of 0.67, 1.06, and 1.41 mmol/g were achieved for D_{KOH} exposed to 10, 30, and 50 vol% CO_2 at 50 °C, respectively. The Langmuir adsorption isotherm model thoroughly describes the effectiveness of CO_2 adsorption on carbon-based adsorbents at low temperature and high CO_2 partial pressure. Raising the CO_2 concentration in the inlet gas increases the interaction between CO_2 and the adsorbent particles, resulting in enhanced CO_2 adsorption. Moreover, due to the exothermic nature of the physisorption process, the decrease in the amount of captured CO_2 ensues from the increase in adsorption temperature. According to the higher CO_2 uptake of D_{KOH} at 25 °C and under 90 vol% of CO_2, these conditions were selected to further analyze the capture performance of the samples upon cycling.

3.2.2. Comparison of CO_2 capture activity of the samples

Fig. 7 presents the mass gain (wt%) for CAC, D, and D_{KOH} during three adsorption/desorption cycles under the aforementioned experimental conditions (T = 25 °C and 90 vol% CO_2). The synthesized adsorbent activated by KOH showed superior CO_2 uptake values in each cycle compared to the other two samples. A better CO_2 uptake potential was reported for the raw D sample than for the commercial AC. During three consecutive cycles, an average CO_2 uptake of 1.37 and 1.59 mmol/g were acquired for CAC and D respectively, indicating approximately 16% better performance of D sample from produced from date seeds. The D_{KOH} adsorbent captured CO_2 reaching an average capacity of 2.66 mmol/g, leading to a 94 and 67.2% enhancement in the average CO_2 capture capacity compared to CAC and D, respectively. Accordingly, both synthesized adsorbents, raw and activated samples, indicated higher CO_2 capture than CAC. Among the date seeds-derived samples, D and D_{KOH}, the superior adsorption capacity was acquired for the KOH-promoted sample. The utilization of chemical modification results in a 67.3% increase in average uptake potential. Based on the reported CO_2 uptake activity and textural features (pore volume and surface area) for CAC, D, and D_{KOH}, it can be noted that there is a high conformity between their porosity and uptake capacity, in which; the more porous

Table 4
TGA results for samples CAC, D, and D_{KOH} within three cycles at adsorption temperature of 25 °C and desorption temperature of 120 °C and 90 vol% CO_2 concentration in the feed gas.

Sample	Uptake	CO_2 adsorption capacity			
		Cycle 1	Cycle 2	Cycle 3	Average
CAC	wt%	6.038	6.013	6.029	6.03
	mmol/g	1.372	1.367	1.37	1.37
D	wt%	7.136	6.997	6.851	7.00
	mmol/g	1.622	1.59	1.557	1.59
D_{KOH}	wt%	11.749	11.653	11.7	11.70
	mmol/g	2.67	2.648	2.659	2.66

texture of D_{KOH} compared to CAC and D increased to accessible adsorptive sites and enhancement in the amount of captured CO_2. Based on the TGA cyclic experiments, D_{KOH} maintained 99.5% of the initial CO_2 uptake after three cycles.

3.3. Fluidization assessment

The agglomeration of nanoparticles adversely affects the efficiency of chemical processes [64–66]. CO_2 capture through solid adsorbents requires an aggregate-free and homogeneous stream of nanoparticles to enhance the efficiency of solid adsorbents. TGA analysis cannot address the gas-solid contact and the heat/mass transfer quality between the gas and solid particles, the main parameters affecting the CO_2 capture efficiency in fluidized bed reactors. In addition to improving CO_2 sorption potential, boosting the fluidity of ACs is required to industrialize them for pilot-scale applications. Pointing to the utilization of fluidized bed reactors for CO_2 capture purposes the fluidization behavior of the ACs was evaluated at room temperature. Even though fluidized bed reactors operate under the fast fluidization regime in realistic conditions, assessing the fluidization behavior of ACs in a lab-scale fluidized bed at low gas velocities (of the order of cm/s) is highly beneficial to determining their fluidity quality and the effectiveness of the considered improvement method.

3.3.1. Fluidity of pure adsorbents

The bed expansion ratios of D and D_{KOH} during the fluidization tests under a gas velocity ranging from 1 to 4 cm/s are plotted in Fig. 8. There is an identical bed expansion trend for D and D_{KOH} characterized by agglomerate bubbling fluidization (ABF) due to the formation of several bubbles across the bed during their fluidization. Based on the visual observation, exerting a higher downward-flowing gas velocity that, in turn, applies more drag force could not overcome the formation of gas bubbles and channels for these sorbents. As presented in Fig. 8, the bed expansion ratio of D_{KOH} increased from 1.45 to 2.44 with a slighter slope when the gas velocity increased from 1 to 3.9 cm/s. The increment in gas velocity leads to an increase in the applied drag force by inlet gas, which can reduce the inter-particle adhesion forces to homogenize the fluidizability.

To validate the visual conclusion about the fluidization quality of date seeds-derived ACs, the Richardson-Zaki eq. (R-Z) was utilized. This equation establishes a linear relation between the inlet gas velocity (U_g), the terminal velocity (U_t), and the bed voidage (ε_b) for nanoparticle agglomerates as follows:

$$\text{Log } U_g = \text{Log } U_t + n \text{ Log } \varepsilon_b \quad (4)$$

n is the R-Z's index that interprets the fluidity quality. ε_b is determined as follows:

$$\varepsilon_b = 1 - \frac{(1-\varepsilon_{b_0})}{\left(H/H_0\right)} \quad (5)$$

where H_0 and H are addressed to the bed heights at zero and the considered gas velocity, respectively. Based on the presented data in [16,67], an initial bed voidage (ε_{b_0}) value of 0.25 was chosen for the ACs-derived adsorbents in this research. With Log U_g being plotted against Log ε_b in Fig. 8, the n index of D and D_{KOH} were acquired and are summarized in Table 5. The n index of 5 distinguishes two regions in the fluidity behaviors: agglomerate bubbling fluidization (ABF) shows n index <5 whereas values of n index >5 correspond to agglomerate particulate fluidization (APF), characterized by a uniform and bubbles-less flowability regime.

Table 5
Fluidity characteristics of D, D_{KOH}, and $S_{2.5}D_{KOH}$.

Sorbent	H/H_0 (at U_g of ~ 4 cm/s)	n index	Fluidization quality
D	2.22	2.55	ABF
D_{KOH}	2.5	3.96	ABF
$S_{2.5}D_{KOH}$	3.62	6.76	APF

Based on the optical visualization (see Fig. 9), the ACs adsorbents showed bubble- and channel-containing fluidization regimes associated with the fluctuated surface, hindering the expansion of particles exposed to the gas velocity of ~3.5 cm/s. It is worth noting that the higher bed expansion of ACs at gas velocities above 3 cm/s can be attributed to partial fluidization. Additionally, the elutriation of particles was observed in agreement with the calculated fluidization parameters. It corroborates the ACs belonging to the Geldart C category. As a result, according to the tabulated data presented in Table 5, D and D_{KOH} showed ABF behavior, revealing the necessity of improving their fluidity performance toward industrialization.

3.3.2. Fluidity of physically modified adsorbents

As previously mentioned, inter-particle forces cause adherence of the fine particles to each other, leading to a sensitive decrease in gas-solid contact surface area, bed expansion during fluidization, and consequently, CO_2 uptake. The physical mixing of cohesive particles with fluidizable auxiliary materials to significantly diminish internal forces between particles has been recognized as an efficient approach. In the current study, D_{KOH} was mixed with 2.5 wt% hydrophobic nano silica via the dry hand-mixing method, aiming to improve the fluidity performance of D_{KOH}. SEM images of the silica-coated ACs ($S_{2.5}D_{KOH}$) and D_{KOH} are illustrated in Fig. 3c and d, respectively. The added SiO_2 NPs well distributed on the D_{KOH} surface, demonstrating the high quality of the physical modification of the adsorbent. A comparison of these two adsorbents indicates the reduction in surface-located accessible AC particles to capture CO_2 molecules and a decrease in morphological porosity. As reported in Table 2, a BET surface area value of 545.95 m^2/g for $S_{2.5}D_{KOH}$ was approximately 8% lower than that of D_{KOH} (595.94 m^2/g). Moreover, a 23.32% decrease in pore volume ensued from coating D_{KOH} with 2.5 wt% SiO_2 NPs. The coverage of accessible surfaces and the occlusion of textural pores with added SiO_2 NPs are the reasons behind the abovementioned reductions in free surface area and pore volume, respectively. On the other hand, mixing the D_{KOH} particles with SiO_2 NPs hinders the particles' agglomeration during fluidization by diminishing the inter-particle cohesion. Accordingly, it is expected that the physical mixing of D_{KOH} with hydrophobic SiO_2 NPs affects both the fluidizability and CO_2 capture performance of D_{KOH}.

Regarding our previous studies, we found that removing dense agglomerates of SiO_2 NPs and reducing their sizes results in more contact interaction between the surface of the host (sorbent) and guest particles (SiO_2). In turn, it leads to the homogenous mixing of the particles and appropriate fluidization behavior [68]. According to our investigations, reducing the size of SiO_2 particles as auxiliary additives decreases the van der Waals adhesion forces between cohesive sorbent particles [16,42,69]. Hence, in the present study, hydrophobic SiO_2 NPs were sieved to particle sizes of ~150 μm. The fluidization of $S_{2.5}D_{KOH}$ under different gas velocities was analyzed and is depicted in Fig. 8. There is a considerable enhancement in bed expansion of $S_{2.5}D_{KOH}$ compared to D_{KOH}. As reported in Table 1, in the presence of 2.5 wt% SiO_2 NPs, the bed expansion of D_{KOH} increased ~45% at a gas velocity of ~4 cm/s. The plotted R-Z equation indicated an n index of 6.76 for $S_{2.5}D_{KOH}$, which corroborates its APF quality (see Fig. 8b). Having reduced the inter-particle adhesion noticeably, the added 2.5 wt% SiO_2 NPs showed great effectiveness on the flowability of D_{KOH} particles, resulting in an excellent bed expansion value of 3.6 at a gas velocity of ~4 cm/s. For a better perception, a snapshot of $S_{2.5}D_{KOH}$ during fluidization at 3.5 cm/s is presented in Fig. 9. The image illustrates more particle expansion in the case of $S_{2.5}D_{KOH}$ during fluidization compared to D_{KOH}, which matches the data reported in Fig. 8. Based on the visual observation and Fig. 9, the fluidized regime of $S_{2.5}D_{KOH}$ consists in a bubble-less homogenous bed without formation of gas channels where bed expansion

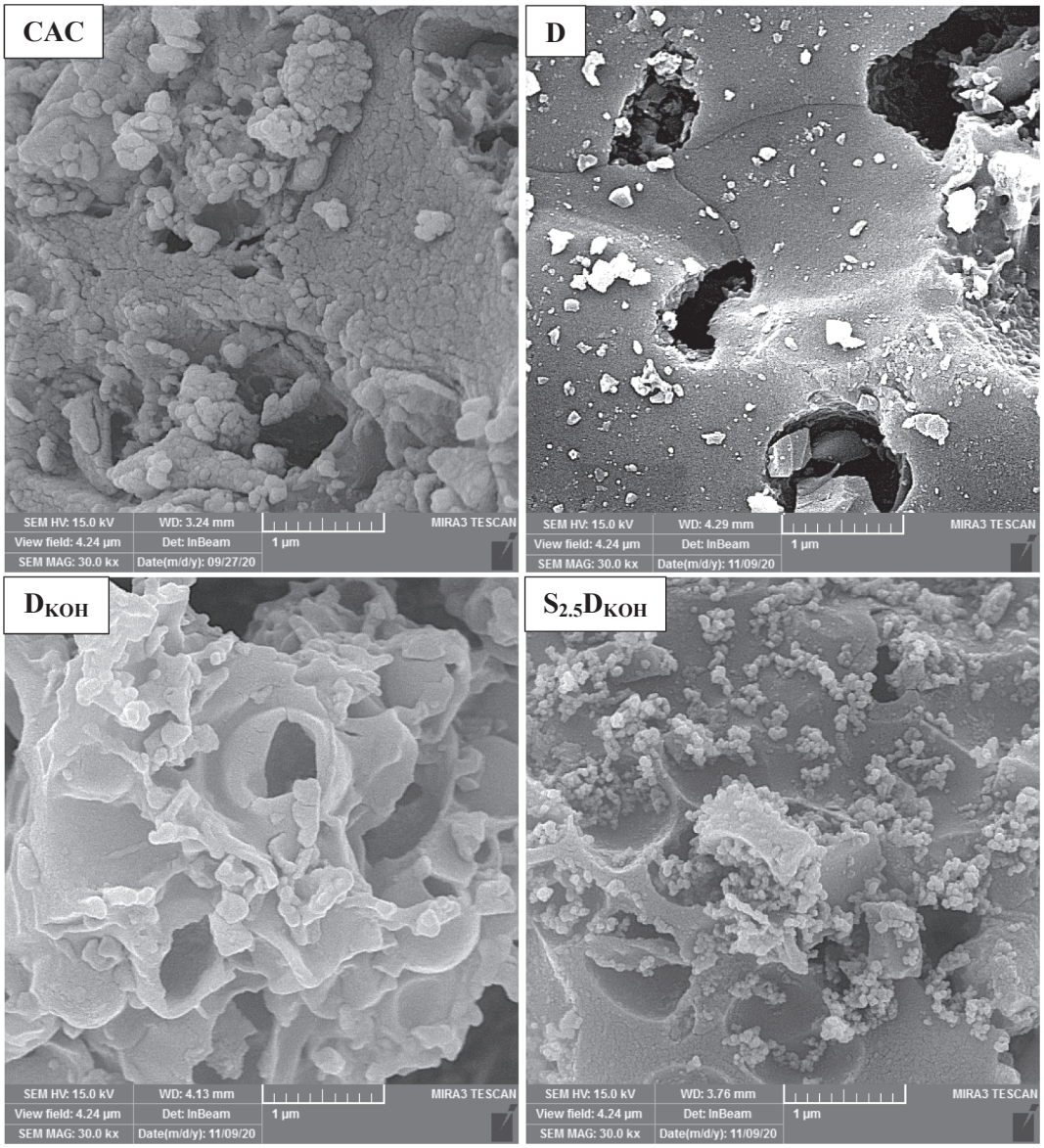

Fig. 3. SEM images of CAC, D, D_{KOH} and $S_{2.5}D_{KOH}$.

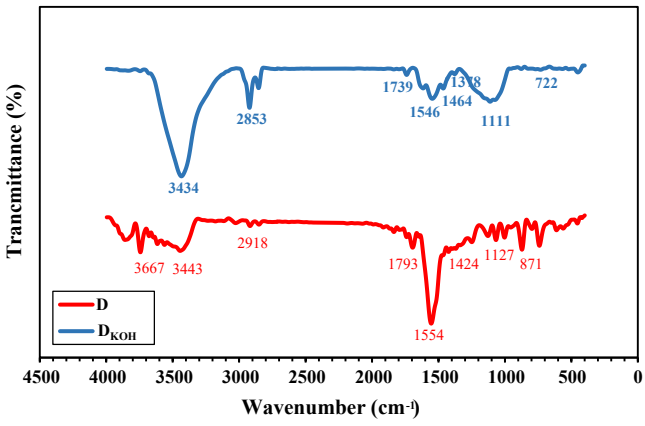

Fig. 4. FTIR spectra of D and D_{KOH}.

is significantly enhanced.

3.4. CO_2 capture activity of D_{KOH} and $S_{2.5}D_{KOH}$

D_{KOH} adsorbent was analyzed over 25 consecutive adsorption/desorption cycles to evaluate its large-scale implementation efficiency at relevant industrial conditions. The adsorption stage was performed under a gas flow containing 15 vol% CO_2 balanced with N_2 for 60 min at 25 °C, and the temperature was increased to 120 °C during the desorption stage. The test was carried out twice to ensure the experiment's reproducibility, and the average uptake was calculated and is illustrated in Fig. 10. The initial CO_2 uptake of D_{KOH} increased from 1.251 to 1.28 after three cycles and then progressively reduces to reach 1.259 mmol/g in the fifth cycle. Overall, the CO_2 uptake keeps stable upon cycling, with a standard deviation between cycles of <0.0119 mmol/g. A durability of 100% during 25 successive adsorption-desorption cycles for D_{KOH} corroborates the effectiveness of chemical activation of D, comparable with other synthesized samples reported in the literature. For instance, synthesized ACs derived from oil sands coke retained 86% of its primary sorption potential within 15 consecutive cycles at 50 °C under 66.6 vol% CO_2. Compared with our previous work,

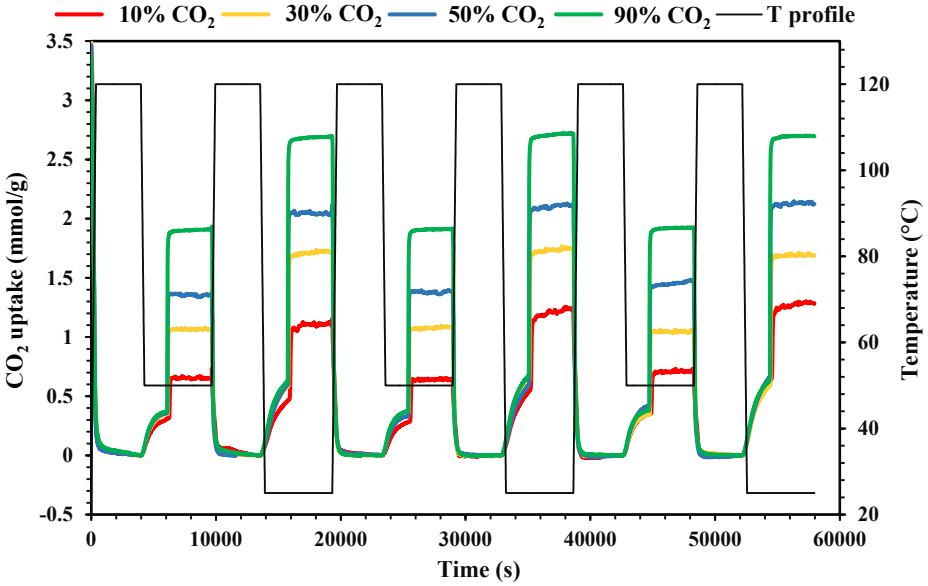

Fig. 5. TGA profiles for D_{KOH} at adsorption temperatures of 25 and 50 °C and desorption temperature of 120 °C in the presence of 10, 30, 50, and 90 vol% CO_2, N_2 balance.

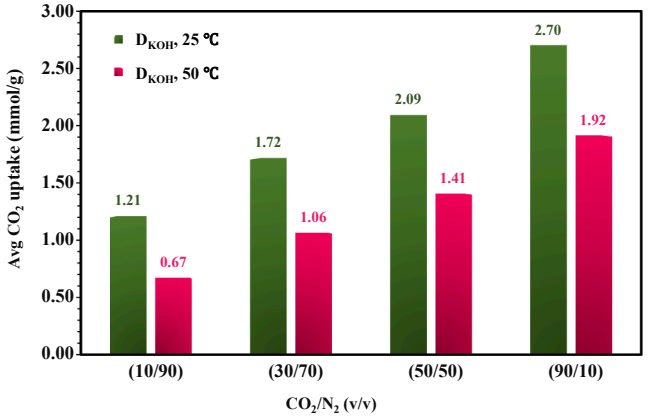

Fig. 6. Average CO_2 uptake of D_{KOH} within three cycles at adsorption temperatures of 25 and 50 °C and desorption temperature of 120 °C in the presence of 10, 30, 50, and 90 vol% CO_2, N_2 balance.

D_{KOH} also demonstrated superior stability to a synthesized carbon nanotube (CNT) [16,70], which endured 9% deactivation under the same experimental conditions applied in this work.

Although using silica nanoparticles improved the fluidization behavior of D_{KOH}, addressing their effect on the CO_2 uptake of the final adsorbent is also a key issue. To investigate the effect of mixed 2.5 wt% SiO_2 on the cyclic activity of D_{KOH}, $S_{2.5}D_{KOH}$ was also analyzed in the TGA tests over 25 consecutive adsorption/desorption cycles in the presence of 15 vol% CO_2 balanced with N_2 at 25 °C. The cyclic activities are summarized in Table 6. The measured CO_2 capture capacities of D_{KOH} and $S_{2.5}D_{KOH}$ depicted in Fig. 10. There is a slight decrease in CO_2 uptake and cyclic durability of $S_{2.5}D_{KOH}$ compared to D_{KOH}. When D_{KOH} is mixed with 2.5 wt% SiO_2, the CO_2 uptake reduced from approximately 1.26 mmol CO_2/ g adsorbent to around 1.16 mmol CO_2/ g adsorbent which accounts for an 8% reduction. There is an adverse influence of the addition of fluidizable SiO_2 NPs on the morphological porosity of the sample. Considering the reported surface and pore volume data in Table 2, $S_{2.5}D_{KOH}$ presents lower surface area (545.95 m^2/g) and pore volume (0.364 cm^3/g) compared to D_{KOH} (595.94 m^2/g and 0.475 cm^3/ g, respectively). It can be concluded that mixing the synthesized adsorbent with silica nanoparticles may jeopardize the access of the CO_2 molecules; however, it mitigates inter-particle adhesion forces and inhibits the agglomeration of adsorbent particles improving gas-solid contact area. On the other hand, both D_{KOH} and $S_{2.5}D_{KOH}$ showed high CO_2 uptakes and outstanding cyclic sorption durability after 25 cycles, demonstrating the formation of highly thermal-robust carbon-based and easy-fluidizable adsorbents for the CO_2 capture process. It is worth noting that the assessment of SiO_2 influence on cyclic performance should be conducted in fluidized bed systems for an engineering-based comparison, and it is considered the main target of our forthcoming research.

3.5. Benchmarking with available literature

The CO_2 uptake of D_{KOH} and $S_{2.5}D_{KOH}$ adsorbents developed in this work are summarized and compared with data available in the literature for ACs-based adsorbents tested under similar conditions (see Table 7). This comparison obviously reveals that the developed KOH-promoted ACs are among the best adsorbents for CO_2 capture in terms of CO_2 uptake compared with the state-of-the-art. A vital issue that should also be addressed is related to the cost of the manufactured adsorbents. For instance, even though slightly higher sorption potentials were reported in the cases of glucose [50] and *Camellia japonica* [60], the KOH-modified sorbents were prepared from the waste material with broad availability in the Middle East. In light of this, it can be stated that the developed adsorbents from date seeds can be labeled as environmentally friendly and economical. As a result, considering the environmental aspects of engineering, D_{KOH} seems more suitable according to the simplicity of the productive properties. On the other hand, the fabrication of a fluidizable sorbent at the expense of a reduction in CO_2 uptake still needs to be addressed in representative conditions to trade off the substantial improvement in fluidity quality and CO_2 capture performance. As previously mentioned, all data gathered in Table 7 correspond to studies analyzing the adsorbents in TGA tests, but the CO_2 capture process in fluidized-bed systems needs the development of uniform fluidization to realistically assess the behavior of the CO_2 adsorbents. According to the homogeneous fluidity quality of $S_{2.5}D_{KOH}$ and its CO_2 uptake in the TGA tests, it is expected that the novel developed adsorbent ($S_{2.5}D_{KOH}$) demonstrates superior CO_2 uptake in a fluidized-bed system. In sum, the development of carbon-based adsorbent derived from waste-based date seeds and easy-to-fluidized SiO_2 NPs

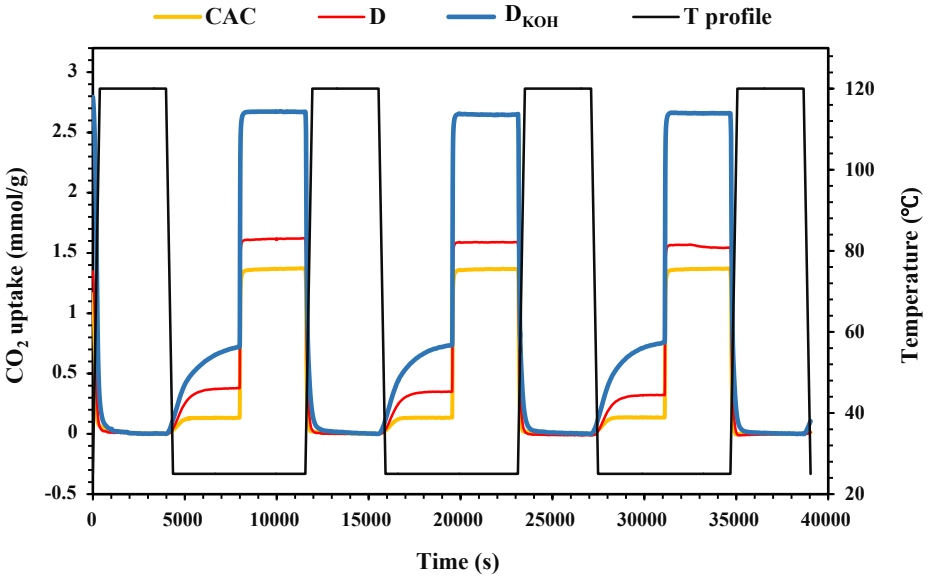

Fig. 7. TGA profiles for CAC, D, and D_{KOH} at adsorption temperature of 25 °C and desorption temperature of 120 °C in 90 vol% CO_2, balance N_2.

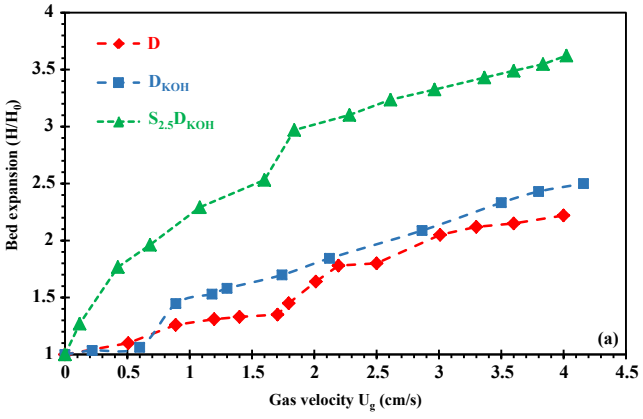

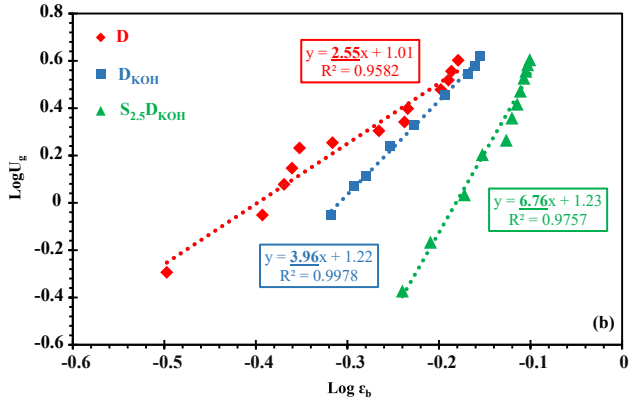

Fig. 8. (a) Bed expansion curves and (b) plot of Log U_g versus log ε_b according to the linear form of the R–Z's equation for D, D_{KOH}, and $S_{2.5}D_{KOH}$ fluidized in dry N_2.

leads to novel nanocomposites with substantial adsorption potential in TG analysis and homogeneous fluidization behavior. The next step in our investigation is the scaling-up of the fluidizable AC adsorbent synthesized in the current study and evaluation in a fluidized-bed system under industrially relevant conditions. According to the facile preparation route of ACs and low-cost materials employed in this work, we do

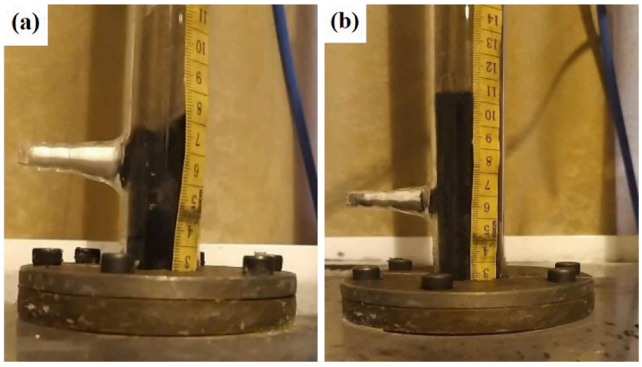

Fig. 9. Snapshots of (a) D_{KOH}, and (b) $S_{2.5}D_{KOH}$ during fluidization at 3.5 cm/s of gas velocity.

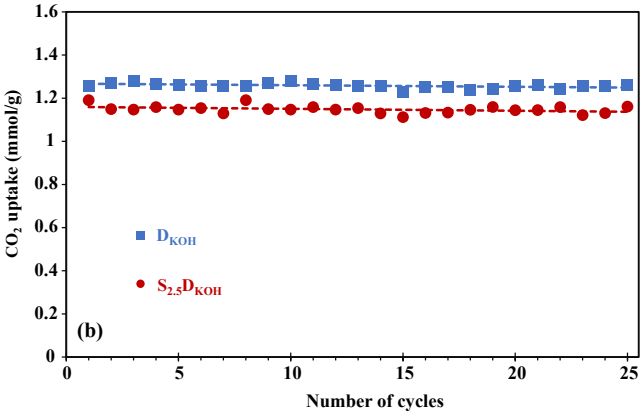

Fig. 10. TGA cyclic tests of D_{KOH} and $S_{2.5}D_{KOH}$ during 25 successive cycles at an adsorption temperature of 25 °C and desorption temperature of 120 °C in 15 vol% CO_2, N_2 balance in terms of CO_2 uptake.

Table 6
Cyclic activity of D_{KOH} and $S_{2.5}D_{KOH}$ within 25 cycles at adsorption temperature of 25 °C and desorption temperature of 120 °C in 15 vol% CO_2 concentration.

Sample	Amount of CO_2 uptake (mmol/g)					Average CO_2 uptake (mmol/g)		Sorption durability (%)		Standard deviation (mmol/g)
	1st cycle	8th cycle	15th cycle	20th cycle	25th cycle	For 5 cycles	For 25 cycles	For 5 cycles	For 25 cycles	For 25 cycles
D_{KOH}	1.251	1.255	1.228	1.255	1.261	1.265	1.258	100	100	0.012
$S_{2.5}D_{KOH}$	1.19	1.149	1.112	1.143	1.161	1.158	1.148	96	98	0.018

Table 7
Comparison of the multi-cyclic performance of ACs tested for low-temperature low partial pressure CO_2 adsorption.

AC source	Scheme	CO_2 capture conditions		Average CO_2 uptake (mmol/g)	Ref.
		Temp. (°C)	CO_2 concentration (vol %)		
Glucose	The AC was activated by KOH with KOH:AC wt. ratio of 1:1 at 800 °C for 1.5 h	25	15	1.44	[50]
Black locust	The AC was prepared from the pyrolysis at 650 °C for 3 h	25	15	0.75	[54]
Black locust	The AC was activated by KOH with KOH:AC wt. ratio of 6:1 at 830 °C for 1.5 h	25	15	1.21	[54]
Jujun grass	The AC was activated by KOH with KOH:AC wt. ratio of 4:1 at 800 °C for 1.5 h	25	15	0.9	[60]
Camellia japonica	The AC was activated by KOH with KOH:AC wt. ratio of 4:1 at 700 °C for 1.5 h	25	15	1.5	[60]
Phenolic resin	The AC was activated by PVA at 800 °C for 1 h	30	15	0.73	[71]
Phenolic resin	The AC was activated by HNO_3 at 25 °C for 1 h	30	15	0.91	[71]
Date seed	The AC was activated by KOH with KOH:AC wt. ratio of 4:1 at 800 °C for 1.5 h	30	15	1.26	This study
Date seed	The KOH-promoted AC was mixed with 2.5 wt% easy-fluidizable SiO_2	25	15	1.19	This study

not anticipate considerable issues related to industrialization and the cost of the environmentally friendly date seeds-based ACs.

3.6. Outlooks

Despite the significant CO_2 uptake activity of modified AC powders reported by TGA analysis and their homogeneous fluidity behavior, the elutriation and attrition of nanoparticles in fluidized beds performing under realistic streams should be addressed as the most challenging issue [72,73]. Improving the mechanical strength of adsorbents is required to alleviate elutriation in fluidized-bed reactors. The granulation of solid adsorbents through various techniques, including extrusion-spheronization [74], rotation-pelletization [75], and extrusion [76], have been proposed to boost the mechanical strength and anti-attrition of solid adsorbents. Hence, the engineering aspects of applying the AC-based adsorbent in an industrial plant necessitate significantly enriching the anti-attrition properties and mechanical strength of AC-based granules. Targeting to develop practical AC-based adsorbents, the granulation of the novel fabricated AC-based adsorbent has been considered as the next step.

4. Conclusions

In the present study, date seeds-derived activated carbons were fabricated through pyrolysis at high temperatures and then activated via the KOH-incorporating method. Commercial AC was also employed as a benchmark sample for comparison and assessing the multicyclic sorption performance of the synthesized ACs. Performed analyses depicted that the chemically AC sample had smaller pores with an average pore diameter of 2.217 nm. Analyzed by the BET/BJH method, this sample showed a surface area of 595.94 m^2/g and pore volume of 0.475 cm^3/g. Superior CO_2 capture performance, including an average CO_2 uptake potential of 2.659 mmol/g in 90 vol% CO_2, was reported for the KOH-promoted AC during three consecutive adsorption-desorption cycles, 67.23 and 94% higher than pyrolyzed date kernel and commercial ACs. The sorption stability of the KOH-promoted AC was evaluated in 25 consecutive adsorption-desorption cycles under 15 vol% CO_2, reproducing industrial capture conditions. A remarkable sorption endurance of up to 100% was recorded for the synthesized samples. Lab-scale fluidization tests under low gas velocities, announced that combining the developed AC with easily fluidizable SiO_2 NPs is a highly efficient strategy to boost its flowability. It was depicted that adding 2.5 wt% of SiO_2 NPs to the KOH-promoted AC caused a 45% increase in the bed expansion ratio at the gas velocity of 4 cm/s and completely homogenized its fluidization behavior, changing the fluidization regime from ABF to APF.

CRediT authorship contribution statement

Milad Iranvandi: Investigation, Methodology. **Maryam Tahmasebpoor:** Supervision, Project administration, Conceptualization. **Babak Azimi:** Formal analysis, Writing – original draft. **Mohammad Heidari:** Formal analysis, Writing - original draft. **Covadonga Pevida:** Conceptualization, Writing – review & editing.

Declaration of Competing Interest

The authors declare that they have no known competing financial interests or personal relationships that could have appeared to influence the work reported in this paper.

Data availability

The authors are unable or have chosen not to specify which data has been used.

Acknowledgements

The authors acknowledge funding from CSIC through the i-COOP 2021 program (Ref. COOPA20492).

References

[1] M. Heidari, M. Tahmasebpoor, S.B. Mousavi, C. Pevida, CO_2 capture activity of a novel CaO adsorbent stabilized with (ZrO_2+Al_2O_3+CeO_2)-based additive under mild and realistic calcium looping conditions, J. CO2 Utiliz. 53 (2021), 101747.

[2] M. Ashrafi, S.B. Mousavi, S. Zeinali Heris, M. Heidari, M. Mohammadpourfard, H. Aslani, Investigation of H_2O_2/UV advanced oxidation process on the removal rate of coliforms from the industrial effluent: a pilot-scale study, Int. J. Hydrog. Energy 47 (78) (2022) 33530–33540.

[3] L. Keshavarz, M.R. Ghaani, J.M.D. MacElroy, N.J. English, A comprehensive review on the application of aerogels in CO_2-adsorption: materials and characterisation, Chem. Eng. J. 412 (2021), 128604.

[4] B. Azimi, M. Tahmasebpoor, P.E. Sanchez-Jimenez, A. Perejon, J.M. Valverde, Multicycle CO_2 capture activity and fluidizability of Al-based synthesized CaO sorbents, Chem. Eng. J. 358 (2019) 679–690.

[5] M. Heidari, S.B Mousavi, F. Rahmani, P.T Clough, S. Ozmen, The novel Carbon Nanotube-assisted development of highly porous CaZrO3-CaO xerogel with boosted sorption activity towards high-temperature cyclic CO2 capture, Energy Conv. Manag. 274 (2022), 116461.

[6] F. Sattari, M. Tahmasebpoor, J.M. Valverde, C. Ortiz, M. Mohammadpourfard, Modelling of a fluidized bed carbonator reactor for post-combustion CO_2 capture considering bed hydrodynamics and sorbent characteristics, Chem. Eng. J. 406 (2021), 126762.

[7] M. Imani, M. Tahmasebpoor, P.E Sánchez-Jiménez, J.M. Valverde, V.M. García, A novel, green, cost-effective and fluidizable SiO2-decorated calcium-based adsorbent recovered from eggshell waste for the CO2 capture process, Sep. Purif. Technol. 305 (2022), 122523.

[8] M. Imani, M. Tahmasebpoor, P.E. Sánchez-Jiménez, J.M. Valverde, V. Moreno, Improvement in cyclic CO_2 capture performance and fluidization behavior of eggshell-derived $CaCO_3$ particles modified with acetic acid used in calcium looping process, J. CO2 Utiliz. 65 (2022), 102207.

[9] X. Wang, K. Zheng, Z. Peng, B. Liu, X. Jia, J. Tian, Exploiting proton masking to protect amino achieve efficient capture CO_2 by amino-acids deep eutectic solvents, Sep. Purif. Technol. 299 (2022), 121787.

[10] Q. Li, H. Wu, Z. Wang, J. Wang, Analysis and optimal design of membrane processes for flue gas CO2 capture, Sep. Purif. Technol. 298 (2022), 121584.

[11] E. Li, Z. Chen, C. Duan, B. Yuan, S. Yan, X. Luo, F. Pan, Z. Jiang, Enhanced CO_2-capture performance of polyimide-based mixed matrix membranes by incorporating ZnO@MOF nanocomposites, Sep. Purif. Technol. 289 (2022), 120714.

[12] M. Heidari, M. Tahmasebpoor, A. Antzaras, A.A. Lemonidou, CO_2 capture and fluidity performance of CaO-based sorbents: effect of Zr, Al and Ce additives in tri-, bi- and mono-metallic configurations, Process. Saf. Environ. Prot. 144 (2020) 349–365.

[13] M. Shen, L. Tong, S. Yin, C. Liu, L. Wang, W. Feng, Y. Ding, Cryogenic technology progress for CO_2 capture under carbon neutrality goals: a review, Sep. Purif. Technol. 299 (2022), 121734.

[14] D. Hospital-Benito, J. Lemus, C. Moya, R. Santiago, C. Paramio, J. Palomar, Aspen plus supported design of pre-combustion CO_2 capture processes based on ionic liquids, Sep. Purif. Technol. 290 (2022), 120841.

[15] Y. Ji, C. Zhang, X.J. Zhang, P.F. Xie, C. Wu, L. Jiang, A high adsorption capacity bamboo biochar for CO_2 capture for low temperature heat utilization, Sep. Purif. Technol. 293 (2022), 121131.

[16] M.J. Nobarzad, M. Tahmasebpoor, M. Heidari, C. Pevida, Theoretical and experimental study on the fluidity performance of hard-to-fluidize carbon nanotubes-based CO_2 capture sorbents, Front. Chem. Sci. Eng. 16 (2022) 1460–1475.

[17] X.-Q. Wang, K.-L. Gao, P. Tan, C. Gu, X.-Q. Liu, L.-B. Sun, Amine-incorporated adsorbents with reversible sites and high amine efficiency for CO2 capture in wet environment, Sep. Purif. Technol. 293 (2022), 121111.

[18] S.M.W. Wilson, High purity CO_2 from direct air capture using a single TVSA cycle with Na-X zeolites, Sep. Purif. Technol. 294 (2022), 121186.

[19] A.S. Palakkal, R.S. Pillai, Evaluating the performance of Cr-Soc-MOF super-adsorbents for CO_2 capture from flue gas under humid condition through molecular simulation, Sep. Purif. Technol. 295 (2022), 121298.

[20] L. Zou, Y. Sun, S. Che, X. Yang, X. Wang, M. Bosch, Q. Wang, H. Li, M. Smith, S. Yuan, et al., Porous organic polymers for post-combustion carbon capture, Adv. Mater. 29 (37) (2017) 1700229.

[21] S. Sun, C. Zhang, S. Guan, S. Xu, P.T. Williams, C. Wu, Ni/support-CaO bifunctional combined materials for integrated CO_2 capture and reverse water-gas shift reaction: influence of different supports, Sep. Purif. Technol. 298 (2022), 121604.

[22] P. Hu, S. Wang, Y. Zhuo, Strengthened CO_2 adsorption over Ce/Al-promoted MgO for fast capture, Sep. Purif. Technol. 287 (2022), 120518.

[23] J. Tian, X. Ding, Q. Wang, Y. Yang, S. Ma, Y. Hou, Z. Huang, L. Liu, Spontaneous formation of nitrogen - doped hierarchical porous microcrystalline Nanosheets with improved CO_2 capture at low and medium pressures, Sep. Purif. Technol. 121809 (2022).

[24] A.S. González, M.G. Plaza, F. Rubiera, C. Pevida, Sustainable biomass-based carbon adsorbents for post-combustion CO_2 capture, Chem. Eng. J. 230 (2013) 456–465.

[25] F. Montagnaro, A. Silvestre-Albero, J. Silvestre-Albero, F. Rodríguez-Reinoso, A. Erto, A. Lancia, M. Balsamo, Post-combustion CO_2 adsorption on activated carbons with different textural properties, Microporous Mesoporous Mater. 209 (2015) 157–164.

[26] R. Javadpour, S.Z. Heris, Y. Mohammadfam, Optimizing the effect of concentration and flow rate of water/ MWCNTs nanofluid on the performance of a forced draft cross-flow cooling tower, Energy 217 (2021), 119420.

[27] N. Karimi Bakhtiyar, R. Javadpour, S.Z. Heris, M. Mohammadpourfard, Improving the thermal characteristics of a cooling tower by replacing the operating fluid with functionalized and non-functionalized aqueous MWCNT nanofluids, Case Stud. Therm. Eng. 39 (2022), 102422.

[28] R. Javadpour, S.Z. Heris, J.P. Meyer, Experimental study of the effect of filled bed type on the performance of a cross-flow cooling tower with the approach of using nanofluids, Energy Rep. 8 (2022) 8346–8360.

[29] J. Sreńscek-Nazzal, K. Kiełbasa, Advances in modification of commercial activated carbon for enhancement of CO_2 capture, Appl. Surf. Sci. 494 (2019) 137–151.

[30] A. Mukherjee, J.A. Okolie, A. Abdelrasoul, C. Niu, A.K. Dalai, Review of post-combustion carbon dioxide capture technologies using activated carbon, J. Environ. Sci. 83 (2019) 46–63.

[31] A.E. Ogungbenro, D.V. Quang, K.A. Al-Ali, L.F. Vega, M.R.M. Abu-Zahra, Physical synthesis and characterization of activated carbon from date seeds for CO_2 capture, J. Environ. Chem. Eng. 6 (4) (2018) 4245–4252.

[32] A.E. Ogungbenro, D.V. Quang, K.A. Al-Ali, L.F. Vega, M.R.M. Abu-Zahra, Synthesis and characterization of activated carbon from biomass date seeds for carbon dioxide adsorption, J. Environ. Chem. Eng. 8 (5) (2020), 104257.

[33] J. Wang, S. Kaskel, KOH activation of carbon-based materials for energy storage, J. Mater. Chem. 22 (45) (2012) 23710–23725.

[34] S.W. Choi, J. Tang, V.G. Pol, K.B. Lee, Pollen-derived porous carbon by KOH activation: effect of physicochemical structure on CO_2 adsorption, J. CO2 Utiliz. 29 (2019) 146–155.

[35] J. Serafin, M. Baca, M. Biegun, E. Mijowska, R.J. Kaleńczuk, J. Sreńscek-Nazzal, B. Michalkiewicz, Direct conversion of biomass to nanoporous activated biocarbons for high CO_2 adsorption and supercapacitor applications, Appl. Surf. Sci. 497 (2019), 143722.

[36] J.M. Salman, V.O. Njoku, B.H. Hameed, Bentazon and carbofuran adsorption onto date seed activated carbon: kinetics and equilibrium, Chem. Eng. J. 173 (2) (2011) 361–368.

[37] N. Abuelnoor, A. AlHajaj, M. Khaleel, L.F. Vega, M.R.M. Abu-Zahra, Activated carbons from biomass-based sources for CO_2 capture applications, Chemosphere 282 (2021), 131111.

[38] H. Mumtaz, M. Farhan, M. Amjad, F. Riaz, A.H. Kazim, M. Sultan, M. Farooq, M. A. Mujtaba, I. Hussain, M. Imran, et al., Biomass waste utilization for adsorbent preparation in CO_2 capture and sustainable environment applications, Sustain. Energy Technol. Assessm. 46 (2021), 101288.

[39] C. Soria-Hoyo, J.M. Valverde, J.R. van Ommen, P.E. Sánchez-Jiménez, L.A. Pérez-Maqueda, M.J. Sayagués, Synthesis of a nanosilica supported CO_2 sorbent in a fluidized bed reactor, Appl. Surf. Sci. 328 (2015) 548–553.

[40] D. Geldart, Types of gas fluidization, Powder Technol. 7 (5) (1973) 285–292.

[41] M. Tahmasebpoor, Y. Rahimvandi Noupoor, P. Badamchizadeh, Fluidity enhancement of hard-to-fluidize nanoparticles by mixing with hydrophilic nanosilica and fluid catalytic cracking particles: experimental and theoretical study, Phys. Fluids 31 (7) (2019), 073301.

[42] M. Tahmasebpoor, R. Ghasemi Seif Abadi, Y. Rahimvandi Noupoor, P. Badamchizadeh, Model based on electrostatic repulsion and hydrogen bond forces to estimate the size of nanoparticle agglomerates in fluidization, Ind. Eng. Chem. Res. 55 (50) (2016) 12939–12948.

[43] N. Rodríguez, M. Alonso, J.C. Abanades, A. Charitos, C. Hawthorne, G. Scheffknecht, D.Y. Lu, E.J. Anthony, Comparison of experimental results from three dual fluidized bed test facilities capturing CO_2 with CaO, Energy Procedia 4 (2011) 393–401.

[44] Y. Rahimvandi Noupoor, M. Tahmasebpoor, A novel internal assistance method for enhanced fluidization of nanoparticles, Korean J. Chem. Eng. 36 (8) (2019) 1377–1387.

[45] J.M. Valverde, A. Perejon, L.A. Perez-Maqueda, Enhancement of fast CO_2 capture by a Nano-SiO2/CaO composite at ca-looping conditions, Environ. Sci. Technol. 46 (11) (2012) 6401–6408.

[46] O. Amjadi, M. Tahmasebpoor, H. Aghdasinia, Fluidization behavior of cohesive ca $(OH)_2$ powders mixed with hydrophobic silica nanoparticles, Chem. Eng. Technol. 42 (2) (2019) 287–296.

[47] G. Sethia, A. Sayari, Comprehensive study of ultra-microporous nitrogen-doped activated carbon for CO_2 capture, Carbon 93 (2015) 68–80.

[48] A. Alabadi, S. Razzaque, Y. Yang, S. Chen, B. Tan, Highly porous activated carbon materials from carbonized biomass with high CO_2 capturing capacity, Chem. Eng. J. 281 (2015) 606–612.

[49] J. Serafin, U. Narkiewicz, A.W. Morawski, R.J. Wróbel, B. Michalkiewicz, Highly microporous activated carbons from biomass for CO_2 capture and effective micropores at different conditions, J. CO2 Utiliz. 18 (2017) 73–79.

[50] Z. Zhang, D. Luo, G. Lui, G. Li, G. Jiang, Z.P. Cano, Y.-P. Deng, X. Du, S. Yin, Y. Chen, In-situ ion-activated carbon nanospheres with tunable ultramicroporosity for superior CO_2 capture, Carbon 143 (2019) 531–541.

[51] M. Li, R. Xiao, Preparation of a dual pore structure activated carbon from rice husk char as an adsorbent for CO_2 capture, Fuel Process. Technol. 186 (2019) 35–39.

[52] M. Idrees, V. Rangari, S. Jeelani, Sustainable packaging waste-derived activated carbon for carbon dioxide capture, J. CO2 Utiliz. 26 (2018) 380–387.

[53] C. Quan, X. Jia, N. Gao, Nitrogen-doping activated biomass carbon from tea seed shell for CO_2 capture and supercapacitor, Int. J. Energy Res. 44 (2) (2020) 1218–1232.

[54] C. Zhang, W. Song, Q. Ma, L. Xie, X. Zhang, H. Guo, Enhancement of CO2 capture on biomass-based carbon from black locust by KOH activation and ammonia modification, Energy Fuel 30 (5) (2016) 4181–4190.

[55] J. Han, L. Zhang, B. Zhao, L. Qin, Y. Wang, F. Xing, The N-doped activated carbon derived from sugarcane bagasse for CO2 adsorption, Ind. Crop. Prod. 128 (2019) 290–297.

[56] H. Wei, S. Deng, B. Hu, Z. Chen, B. Wang, J. Huang, G. Yu, Granular bamboo-derived activated carbon for high CO2 adsorption: the dominant role of narrow micropores, ChemSusChem 5 (12) (2012) 2354–2360.
[57] J. Wang, A. Heerwig, M.R. Lohe, M. Oschatz, L. Borchardt, S. Kaskel, Fungi-based porous carbons for CO2 adsorption and separation, J. Mater. Chem. 22 (28) (2012) 13911–13913.
[58] M. Sevilla, A. Fuertes, B., Sustainable porous carbons with a superior performance for CO2 capture, Energy Environ. Sci. 4 (5) (2011) 1765–1771.
[59] G.K. Parshetti, S. Chowdhury, R. Balasubramanian, Biomass derived low-cost microporous adsorbents for efficient CO2 capture, Fuel 148 (2015) 246–254.
[60] H.M. Coromina, D.A. Walsh, R. Mokaya, Biomass-derived activated carbon with simultaneously enhanced CO2 uptake for both pre and post combustion capture applications, J. Mater. Chem. A 4 (1) (2016) 280–289.
[61] M. Tahmasebpoor, R. Zarghami, R. Sotudeh-Gharebagh, J.R. van Ommen, N. Mostoufi, Dynamic analysis of the scale-up of fluidized beds, Adv. Powder Technol. 28 (10) (2017) 2621–2629.
[62] S. Naghash-Hamed, N. Arsalani, S.B. Mousavi, Facile copper ferrite/carbon quantum dots magnetic nanocomposite as an effective nitro group reduction reaction nano catalyst for reduction of Para-nitroaniline and Ortho-nitroaniline, Nano Futures 6 (4) (2022), 045003.
[63] H. Alizadeh, H. Pourpasha, S.Z. Heris, P. Estellé, Experimental investigation on thermal performance of covalently functionalized hydroxylated and non-covalently functionalized multi-walled carbon nanotubes/transformer oil nanofluid, Case Stud. Therm. Eng. 31 (2022), 101713.
[64] R. Javadpour, S.Z. Heris, Y. Mohammadfam, S.B. Mousavi, Optimizing the heat transfer characteristics of MWCNTs and TiO2 water-based nanofluids through a novel designed pilot-scale setup, Sci. Rep. 12 (1) (2022) 15154.
[65] A. Aghaei Sarvari, S. Zinali Heris, M. Mohammadpourfard, S.B. Mousavi, P. Estellé, Numerical investigation of TiO2 and MWCNTs turbine meter oil nanofluids: flow and hydrodynamic properties, Fuel 320 (2022), 123943.
[66] S.S. Seyedi, M.R. Shabgard, S.B. Mousavi, S.Z. Heris, The impact of SiC, Al_2O_3, and B_2O_3 abrasive particles and temperature on wear characteristics of 18Ni (300) maraging steel in abrasive flow machining (AFM), Int. J. Hydrog. Energy 46 (68) (2021) 33991–34001.
[67] J. Yang, T. Zhou, L. Song, Agglomerating vibro-fluidization behavior of nano-particles, Adv. Powder Technol. 20 (2) (2009) 158–163.
[68] O. Amjadi, M. Tahmasebpoor, Improving fluidization behavior of cohesive ca$(OH)_2$ adsorbent using hydrophilic silica nanoparticles: parametric investigation, Particuology 40 (2018) 52–61.
[69] M.R. Tamadondar, R. Zarghami, K. Boutou, M. Tahmasebpoor, N. Mostoufi, Size of nanoparticle agglomerates in fluidization, Can. J. Chem. Eng. 94 (3) (2016) 476–484.
[70] M.J. Nobarzad, M. Tahmasebpoor, M. Imani, C. Pevida, S.Z. Heris, Improved CO_2 adsorption capacity and fluidization behavior of silica-coated amine-functionalized multi-walled carbon nanotubes, J. Environ. Chem. Eng. 9 (4) (2021), 105786.
[71] N. Sun, C. Sun, J. Liu, H. Liu, C.E. Snape, K. Li, W. Wei, Y. Sun, Surface-modified spherical activated carbon materials for pre-combustion carbon dioxide capture, RSC Adv. 5 (42) (2015) 33681–33690.
[72] Y. Xu, H. Ding, C. Luo, Y. Zheng, Y. Xu, X. Li, Z. Zhang, C. Shen, L. Zhang, Effect of lignin, cellulose and hemicellulose on calcium looping behavior of CaO-based sorbents derived from extrusion-spherization method, Chem. Eng. J. 334 (2018) 2520–2529.
[73] Y. Yang, W. Liu, Y. Hu, J. Sun, X. Tong, Q. Chen, Q. Li, One-step synthesis of porous Li4SiO4-based adsorbent pellets via graphite moulding method for cyclic CO_2 capture, Chem. Eng. J. 353 (2018) 92–99.
[74] J. Sun, W. Liu, Y. Hu, J. Wu, M. Li, X. Yang, W. Wang, M. Xu, Enhanced performance of extruded–spheronized carbide slag pellets for high temperature CO_2 capture, Chem. Eng. J. 285 (2016) 293–303.
[75] V. Manovic, Y. Wu, I. He, E.J. Anthony, Spray water reactivation/pelletization of spent CaO-based sorbent from calcium looping cycles, Environ. Sci. Technol. 46 (22) (2012) 12720–12725.
[76] C. Qin, J. Yin, H. An, W. Liu, B. Feng, Performance of extruded particles from calcium hydroxide and cement for CO_2 capture, Energy Fuel 26 (1) (2012) 154–161.